

Electrical conduction mechanisms of metal / high- T_c superconductor (YBCO) interfaces

L. F. Lanosa,^{1,*} H. Huhtinen,² P. Paturi,² and C. Acha^{1,†}

¹*Laboratorio de Bajas Temperaturas, Departamento de Física, FCEyN, Universidad de Buenos Aires and IFIBA, UBA-CONICET, Pabellón I, Ciudad Universitaria, C1428EHA Buenos Aires, Argentina*

²*Wihuri Physical Laboratory, Department of Physics, University of Turku, FI-20014 Turku, Finland*

(Dated: January 22, 2020)

Abstract

Current-voltage characteristics of Au / $\text{YBa}_2\text{Cu}_3\text{O}_{7-\delta}$ interfaces (Au/YBCO), built on optimally-doped YBCO thin films, grown by pulsed laser deposition, were measured as a function of temperature in the 50 K to 270 K range, for two different resistance states. A non-trivial equivalent circuit model is proposed, which reveals the existence of a highly inhomogeneous scenario composed by two complex layers: one presenting both a non-linear Poole-Frenkel conduction as well as Variable Range Hopping localization effects (probably associated with $\text{YBa}_2\text{Cu}_3\text{O}_6$) mixed with a minor metallic phase, while the other is also composed by a mixture of YBCO with different oxygen contents, where a metallic ohmic phase still percolates. A microscopic description of the effects produced by the resistance switching is given, showing the evolution of carrier traps, localization effects and dielectric behavior for each state. The dielectric behavior is interpreted in terms of a Maxwell-Wagner scenario.

Keywords: Interface Electrical Properties, Resistive Switching, Superconductor, Poole-Frenkel emission, Maxwell-Wagner effect

*Present address: Departamento de Matemática - FCEyN - Universidad de Buenos Aires and IMAS, UBA-CONICET, Pabellón I, Ciudad Universitaria, C1428EHA Buenos Aires, Argentina

†corresponding author (acha@df.uba.ar)

I. INTRODUCTION

In the last years, memory devices based on the resistive switching mechanism (RS), usually called RRAM, have focused great interest of the scientific and technological community due to the potential technological interest in terms of their application on denser non-volatile memories, with lower energy consumption and better resistance to hostile environments. Additionally, their capacity to reproduce logical gates [1] and to simulate synaptic connections [2] opened interesting paths towards the area of electronic circuits, particularly to those that mimic neural networks [3] and even reproduce the electrical behavior of neurons. [4]

Although great advances have been made to understand the physics behind the memory properties of RRAM devices, as for example, the explanation of the non-trivial behavior observed in the resistance hysteresis loops of metal-transition metal oxide bipolar devices by a voltage-enhanced oxygen diffusion model [5], many aspects are still not addressed in order to fully understand the singular properties of these devices. In particular, considering the oxygen migration easiness in these oxides, the existence of defects or inhomogeneities in a real interface is highly probable and may produce a significant effect on their transport properties. Many factors may contribute to that non-uniform spatial oxygen distribution near the interface, which may regulate the final oxygen concentration distribution: the chemical oxygen affinity of the metallic layer, deposited on top of the oxide surface with a certain roughness, as well as the competition between oxygen electromigration, favored in the high resistance zones, and the oxygen diffusion, due to the Fick's law. Within this framework, the knowledge of which are the microscopic factors that determine the electrical conduction properties through these inhomogeneous interfaces can then be exploited by material engineering strategies in order to take full advantage of the resistance switching properties of these devices.

Devices based on metal / YBCO ($\text{YBa}_2\text{Cu}_3\text{O}_{7-\delta}$) probably will not be useful for massive technological applications due to their not obvious integration to the Si-based electronics and to their partial retentivity [6], associated with their high oxygen diffusivity in certain crystallographic directions [7]. Instead, their interest is based in their capacity to shed light on the electrical transport mechanisms through a metal-complex oxide interface, which is a common feature of many memristive interfaces and particularly to improve our knowledge of the electrical transport and dielectric properties of YBCO. Indeed, metal / YBCO devices

have shown interesting bipolar resistive switching properties [8–12], with particular relaxation effects [7, 13], the electrochemical control of YBCO’s carrier density [14] and present some particular characteristics proper of inhomogeneous interfaces. [6, 15–19].

In this paper, our objective is to identify the relevant transport mechanism through the Au / YBCO interface by analyzing its current-voltage (I-V) characteristics at different temperatures, in order to determine its equivalent circuit model and to reveal the temperature dependence of the microscopic factors that regulate each resistive state.

Our results indicate the existence of a mixture of conduction mechanisms, where the nonlinearities, as previously reported [6, 15], come from a Poole-Frenkel emission, dominated by carrier traps on YBCO, in parallel with a variable range hopping ohmic conduction, both in series with a metallic conduction. These results reveal an scenario where the interfacial zone is highly inhomogeneous in terms of the oxygen distribution, leading to a mixture of conducting and isolating zones. In this way, the elements that may produce a colossal dielectric constant are present, as a consequence of the Maxwell-Wagner effect. [20, 21]

II. EXPERIMENTAL DETAILS

Near optimally-doped and fully relaxed YBCO thin films were grown by pulsed laser deposition (PLD) on top of a (100) single crystal STO substrate. The films were deposited by applying 1500 pulses with a growth rate of 0.1 nm/pulse, producing the 150 nm thick layer as earlier confirmed by transmission electron microscopy (TEM) calibrations under the same deposition conditions. [22] Details of their synthesis and characterization can be found elsewhere (see also Suppl. Material) . [23–25]

Metal-YBCO devices were prepared by using stencil lithography to sputter four metallic electrodes on top of the YBCO thin films. The sputtered electrodes have a width of 30 nm, a $0.7 \times 0.7 \text{ mm}^2$ area and a mean separation of 0.4 mm. Gold leads were carefully fixed over them by using silver paint without contacting directly the surface of the YBCO sample. Three of the electrodes were made with Au, while the other with Pt, as depicted in Fig. 1. As previously shown for YBCO ceramic slabs [12] and checked for the YBCO thin films, this particular choice was based in the fact that the Pt/YBCO interfaces have a lower resistance value than the Au/YBCO ones ($R_{Pt} \lesssim R_{Au}/3$), as well as a small RS amplitude. In this way, we may disregard the influence of the Pt/YBCO electrode and proceed as if

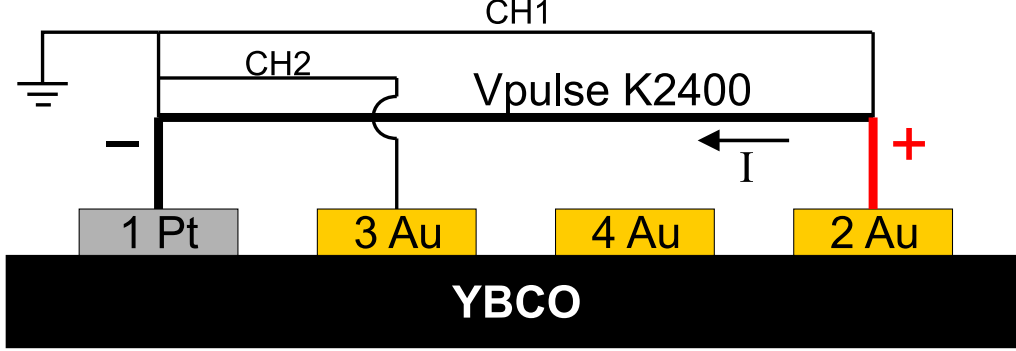


FIG. 1: (Color online) The YBCO thin film device with its electrodes and experimental configuration. Au was sputtered on pads 2-3-4 while Pt on pad 1. Pulses were applied between electrodes "1" (*- polarity*) and "2" (*+ polarity*) with a Keithley 2400 SMU, while a Tektronix 3034 oscilloscope registered voltage drops between pads 2 – 1 in Channel 1 and 3 – 1 in Channel 2.

only the Au/YBCO electrode is active (i.e. presents a relevant RS effect), simplifying the effects produced upon voltage pulsing treatments. Thus, the studied devices correspond to a Pt/YBCO/Au combination, arranged in a planar structure. Pulses were applied between the Pt and Au electrodes, labeled "1" and "2", respectively. The design allowed 3-Wire (3W) and 4-Wire (4W) measurements using the remaining electrodes 3 and 4: 3W to characterize individual metal/YBCO interfaces, and 4W only for the YBCO characterization.

In order to measure the I-V characteristics, 10 ms voltage pulses of increasing amplitude were applied with a Keithley 2400 SMU between electrodes "1" and "2", Pt(-) and Au(+), respectively. This instrument also measure the circulating current (I) during the pulses. A $V_{BIAS} = 0.1V$ pulse is also applied between pulses to control and measure the remnant resistance, R_{REM} . The sketch of the pulsing protocol can be observed in Fig. 2.

At the same time a Tektronix 3034 oscilloscope was used to control the integrity of the applied pulses (Channel 1), and to measure the voltage drop between the Pt electrode "1" and the intermediate Au "3" one (Channel 2). This 3W configuration served to determine the voltage drop in the active "2" Au/YBCO interface for studying its I-V characteristics.

During all the I-V measurements, in order to characterize the same resistive state at different temperatures, the voltage range was carefully limited to avoid the RS of the device. To confirm this, we checked that there were no sudden jumps in R_{REM} during the pulsing protocol.

As shown previously on ceramic YBCO/metal interfaces [12], the thin film YBCO/metal

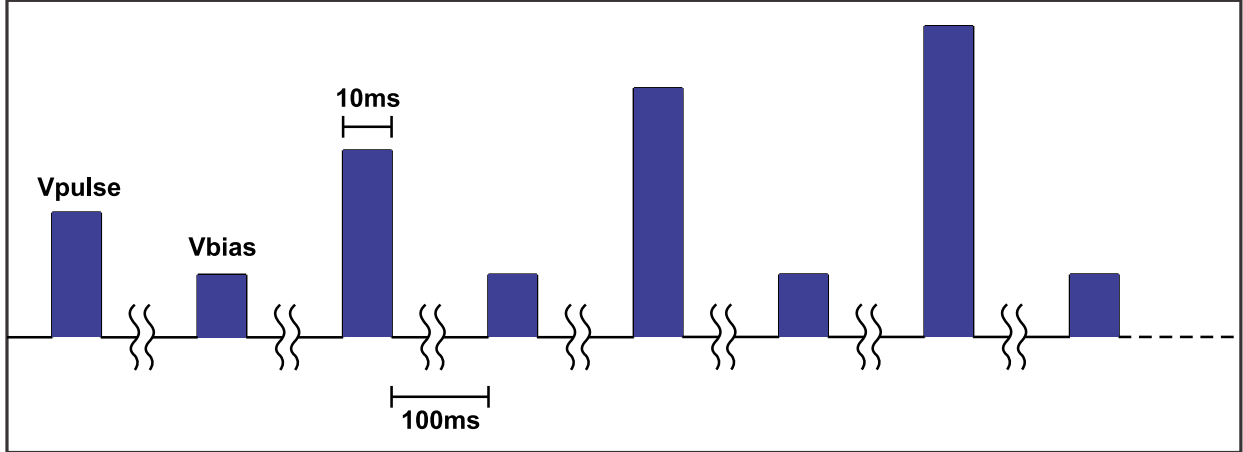


FIG. 2: Diagram of the voltage pulsing protocol used to study the effect of RS on the microscopic parameters that controls the electrical transport properties of the Au/YBCO interface. 10ms pulses (V_{PULSE}) were applied from 0 V to 5 V in 0.1 V steps, with an additional low voltage and fixed 0.1 V pulse (V_{BIAS}) to control and measure the remnant resistance (R_{REM}). Positive polarity pulses were applied for the characterization of the LRS, while negative ones for the HRS.

interface presents a bipolar RS (see Suppl. Material). Briefly, after a certain positive applied pulse [$V_{SET} \sim 5 V @ 270 K$, polarity arbitrarily defined ($-$)Pt/YBCO/Au($+$)], the active Au/YBCO interface sets to a low resistive state (LRS), while after a negative one ($V_{RESET} \sim -5 V @ 270 K$) sets to a high resistive state (HRS).

For each I-V characteristic, temperature was stabilized within a 100 mK range for each selected temperature, varied from 270 K to 50 K at $\sim 5 K$ intervals. Devices were located in a liquid Helium cryostat where temperature was measured using a carbon-glass thermometer, in good thermal contact with the device.

In this way, the device was initially set to the LRS at 270 K ($R_{REM}^{LRS} \simeq 4 k\Omega$). Then its I-V characteristics were measured twice at all the programmed temperatures (on cooling and heating), obtaining similar results in both cases. After stabilizing the temperature at 270 K, the sample was RESET to its HRS ($R_{REM}^{HRS} \simeq 30 k\Omega$) and the same procedure followed to measure the I-V characteristics as a function of temperature for the LRS was completed for the HRS.

The I-V characteristics obtained in the LRS are in the $0V \rightarrow 5V$ range, while in the HRS are in $-5V \rightarrow 0V$. As mentioned, the negative (positive) side in the LRS (HRS) could not be measured in a relevant voltage range in order to avoid a RS.

III. RESULTS AND DISCUSSION

The measured I-V characteristics as a function of temperature for both states (LRS and HRS) can be observed in Fig. 3.

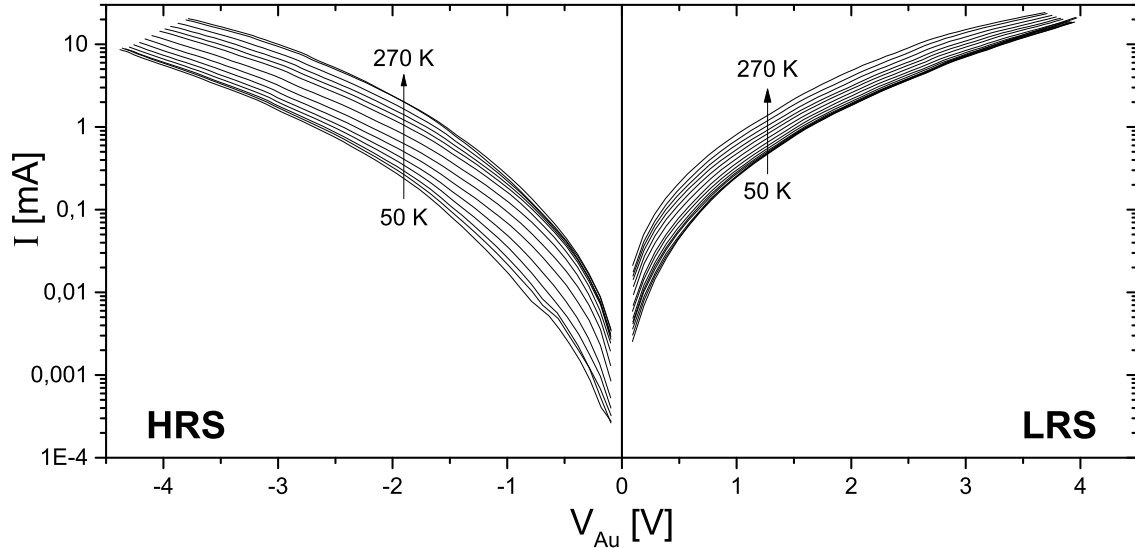


FIG. 3: I-V characteristics of the Au-YBCO interface at different temperatures from 50 K to 270 K for a low (LRS) and a high (HRS) resistance state. For clarity, only curves measured increasing temperature with a $\simeq 15$ K interval are shown.

A systematic increase of the conductivity is observed when increasing the temperature for both states. In the interest of determining if these I-V curves can be associated with a typical interfacial conduction mechanism [26, 27] [i.e. ohmic, Schottky (Sch), Poole-Frenkel (PF), Space Charge Limited Currents (SCLC), Fowler-Nordheim (FN), or to an eventual combination of them], the graphical representation of the I-V curves based on the power exponent $\gamma = d\text{Ln}(I)/d\text{Ln}(V)$ plotted as a function of $V^{1/2}$, can be considered. [28] In fact, this method has proven to be extremely useful in determining the presence of different transport mechanisms when more than one contributes to electric transport. [29–31]

As shown in Fig. 4, despite the noise associated with the calculation of the derivative, it can be observed that γ follows a complex curve, indicating the presence of more than one conduction process. For voltages tending to zero, γ extrapolates to values close to 1 (ohmic), while for intermediate voltages, γ follows a linear-like dependence (Sch or PF), reaching a maximum, with a clear decrease for the higher voltage range (ohmic or SCLC). The

similarity of the curves for both states indicates that the involved conduction mechanisms remain present independently of the RS, which only changes the relative weight of them.

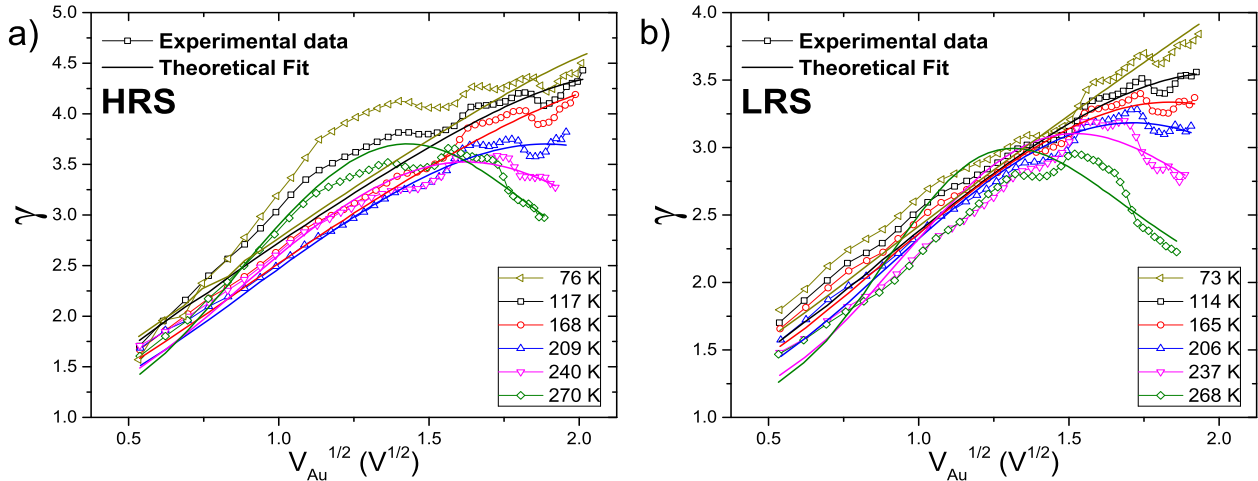


FIG. 4: Experimental and theoretical (see Eq. 3) γ representation of the I-V characteristics for the a) HRS and b) LRS.

As no appreciable rectification was measured a Sch interface can be ruled out. This is in accordance to the fact that ohmic contacts are expected in interfaces where metals with high work function are deposited on p-type oxides. [32] In this way, the most simple equivalent circuit that can be proposed is the one where the non-linear behavior comes from a PF effect, associated with the existence of traps within the oxide, in parallel with a leaky ohmic conduction (R_P), both in series with a limiting ohmic resistor (R_S), probably associated with the conduction through a filamentary YBCO which connects the interfacial zone to the bulk. This equivalent circuit suggests the existence of 2 interfacial regions, as depicted in Fig. 5.

Considering this possible equivalent circuit model suggested by the γ graphical representation of the I-V curves, the following equations can be derived:

$$i_{PF}(v_{PF}) = Av_{PF} \exp[B\sqrt{v_{PF}}], \quad (1)$$

with

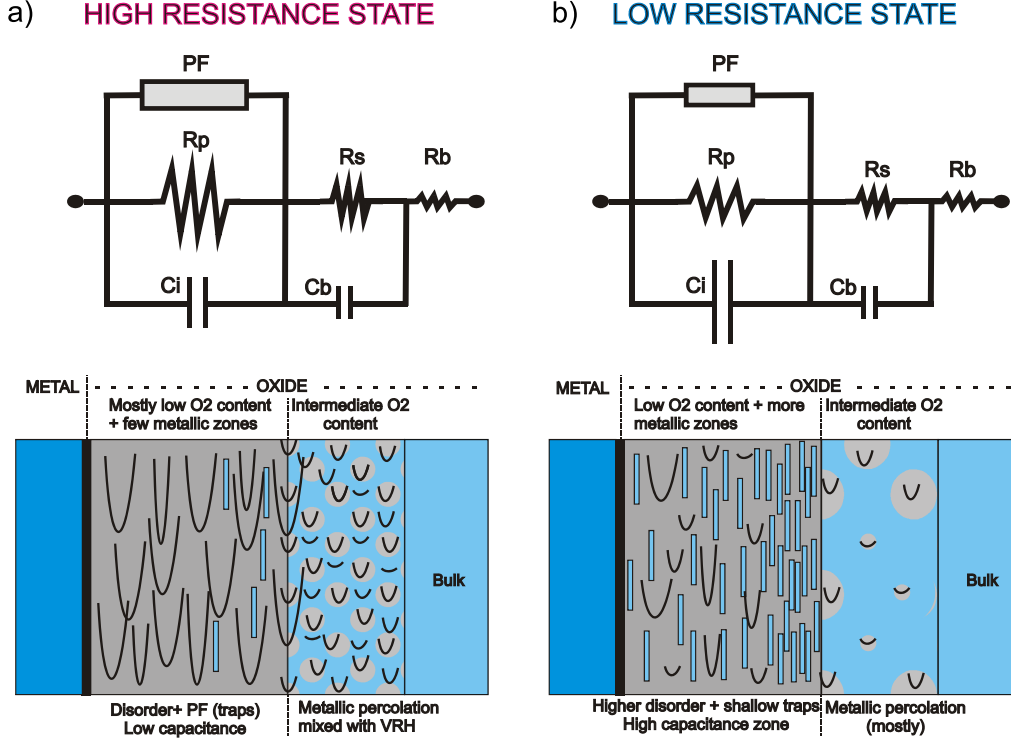


FIG. 5: Schematic of the proposed equivalent circuit model for the Au/YBCO interface at a) HRS and b) LRS. The circuit includes a PF element in parallel with an ohmic resistor (R_P), both in series with a second ohmic resistor (R_S). In this way (see the discussion in the text), the interface is represented by 2 oxygen-depleted regions: the first one, in contact with the metal, mostly composed by YBCO6, where oxygen vacancies act as traps and produce a disordered potential for the electrical carriers (PF+VRH), and the second one, with a lower vacancy content, where the metallic bulk phase still percolates. Notice that the first region also present conducting islands, whose density increases in the LRS, favoring the appearance of Maxwell-Wagner effects.

$$A = \tilde{A}_{PF} \exp \left[\frac{-\bar{\phi}_t}{T} \right] ; \quad B = \frac{q^{3/2}}{k_B T (\pi \epsilon' \epsilon_0 d)^{1/2}}, \quad (2)$$

where i_{PF} and v_{PF} are the current and the voltage across the PF element, respectively. \tilde{A}_{PF} is associated with the geometric factor of the conducting path, the electronic drift mobility (μ) and the density of states in the conduction band. $\bar{\phi}_t$ is the trap energy level (in K), q the electron's charge, k_B the Boltzmann constant, ϵ' the real part of the relative dielectric

constant of the oxide, ϵ_0 the permittivity of vacuum and d the distance associated with the voltage drop v_{PF} . Notice that d is not necessarily equal to the distance between the voltage contacts.

As $v_{PF} = V - v_S = V_{Au} - v_S$, then:

$$I = A(V_{Au} - IR_S) \exp \left[B \sqrt{V_{Au} - IR_S} \right] + \frac{V_{Au} - IR_S}{R_P} \quad (3)$$

Eq. 3 is an implicit equation that should be solved numerically to fit the experimental data. As can be observed in Fig. 6 the experimental I-V characteristics for the HRS and the LRS are very well reproduced by the theoretical representation of the proposed circuit model (Eq. 3), respectively (as well as the corresponding γ curves shown in Fig. 4). A small deviation can be observed at low currents and voltages, probably associated with the existence of low thermoelectric voltages at the interfaces.

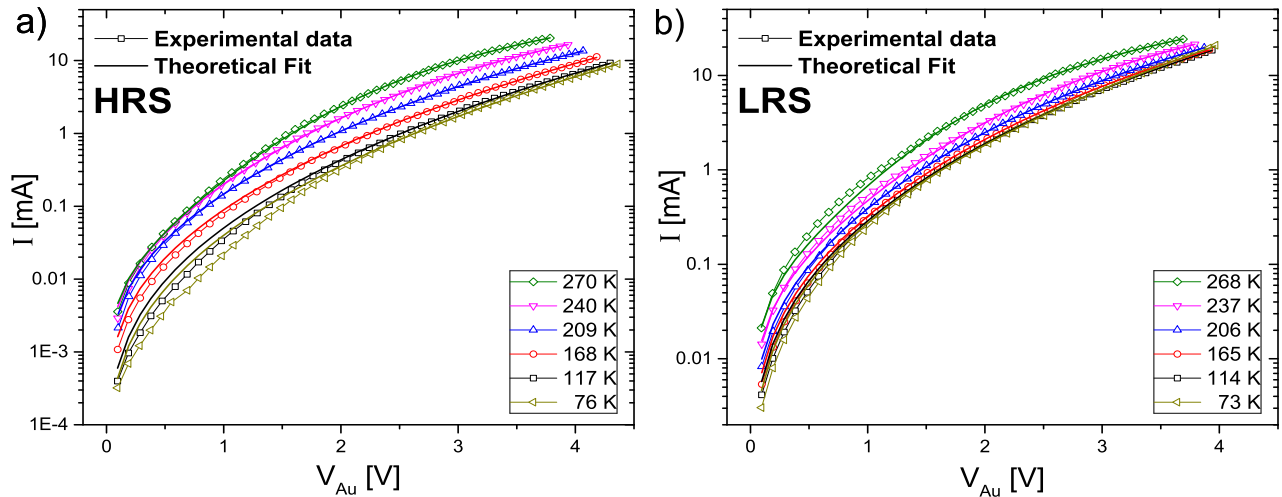


FIG. 6: Experimental and theoretical (Eq. 3) I-V characteristics at different temperatures for the a) HRS and b) LRS.

In this way, the temperature dependence of the fitting parameters R_S , R_P , A and B can be extracted, as shown in Fig. 7-10.

In the LRS, the series resistance R_S mimics the bulk resistance of the YBCO film, with even evidences of its superconducting transition, as can be observed in Fig. 7. As the value of R_S is at least one order of magnitude higher than R_{4W} ($\sim 0.1 \Omega$), we can infer that this is a consequence of a reduced geometric factor, as if the connection of the interfacial

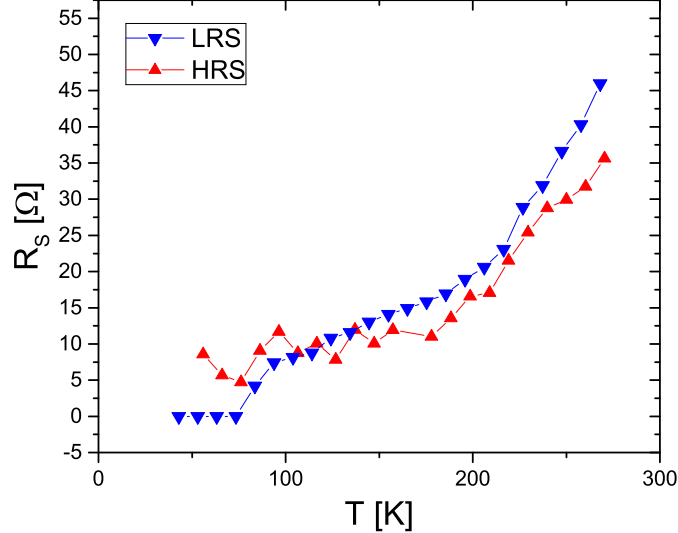


FIG. 7: Series resistance R_S as a function of temperature for the LRS and HRS. A drop to $\simeq 0$ resistance can be observed in the LRS at a temperature close to the superconducting T_c of the bulk YBCO, while this is not the case for the HRS.

zone to the bulk of the film is realized through small conducting channels of near optimally doped YBCO through an insulating matrix of oxygen depleted YBCO. In the HRS, R_S also shows a metallic-like behavior, but no superconducting transition can be detected, probably associated with the disappearance of the percolation of the superconducting state through these still metallic channels.

The existence of the mentioned insulating matrix is revealed by the temperature dependence of R_P . Indeed, as can be observed in Fig. 8, the $R_P(T)$ data is better represented by an Efros-Shklovskii variable range hopping (ES VRH) law ($R_P \sim \exp[(\frac{T_0}{T})^{1/2}]$) rather than by a 2D Mott localization ($R_P \sim \exp[(\frac{T_0}{T})^{1/3}]$), pointing to $\text{YBa}_2\text{Cu}_3\text{O}_x$ with $x \simeq 6$ as the possible phase associated with this particular electric transport. [33, 34]

In fact, the non-linear conduction of $\text{YBa}_2\text{Cu}_3\text{O}_{6+\delta}$ with $\delta < 0.1$ was already reported [33–35] but its origin was not addressed at that time. Here, in accordance to a previous study by Schulman et al. [15], we argue that the oxygen vacancies not only induce disorder, which is at the basis of the electronic localization, but also act as trapping centers, determining an additional non-linear conduction channel based on the PF effect.

By fitting the temperature dependence of the resistivity by the ES VRH law, T_0 was obtained for the HRS and LRS ($\sim 9,000$ K and $14,000$ K, respectively). The localization

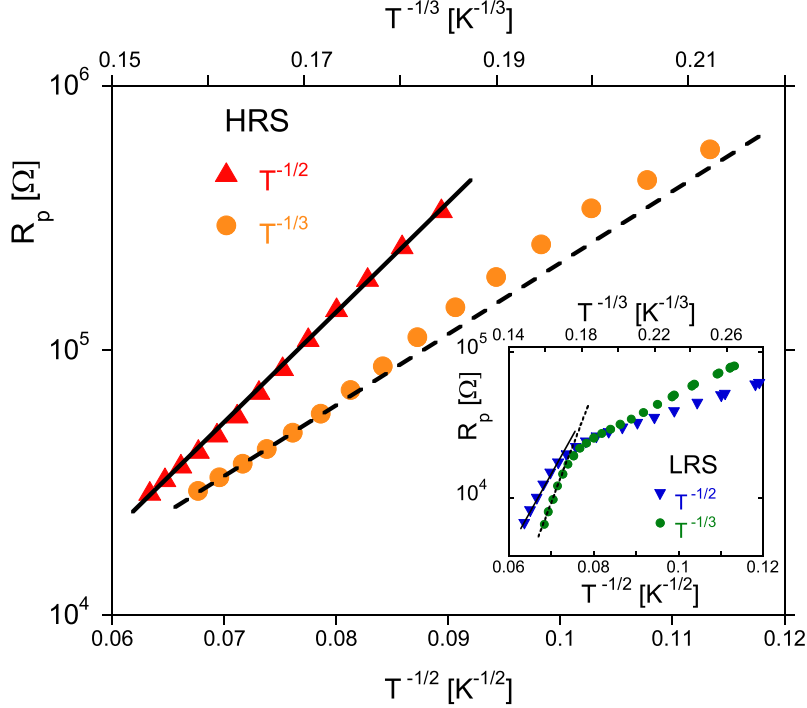


FIG. 8: Parallel resistance R_P as a function of $T^{-1/2}$ and $T^{-1/3}$ for the HRS. The inset shows the same plot for the LRS. Lines are guides to the eye.

length [36, 37] can then be determined as $\xi = 2.8 e^2 / (\epsilon' \epsilon_0 k_B T_0)$. Assuming that $\epsilon' \sim 25$ [38] (see the discussion on ϵ' in the last section of this paper), we obtain that $\xi^{HRS} \simeq 2.6$ nm and $\xi^{LRS} \simeq 1.6$ nm, interestingly indicating that the insulating matrix in the LRS seems to be more disordered than in the HRS. This indicates that when the RS produces the LRS, not only a more conducting path is set but the degree of disorder is increased, probably as a consequence of a noisy distribution of oxygen vacancies.

This insulating phase is present for both the HRS and the LRS (see the inset of Fig. 8) but it can be observed that at low temperatures there is a small increase of the conductance ($T \leq 180$ K and $T \leq 100$ K for the LRS and the HRS (not shown), respectively, consistent with the presence of minor metallic zones.

The temperature dependence of the A parameter, associated with the PF conduction, is shown in Fig. 9 for both HR and LR states. Plotted as $\ln(A)$ vs T^{-1} , a linear dependence with a negative slope can be observed for the HRS in a certain temperature range. According to Eq. 2 this slope represents the mean energy of the PF traps ($\bar{\phi}_t \simeq 270$ K). This value, which depends on the HRS attained, is in the order of magnitude of the ones reported for

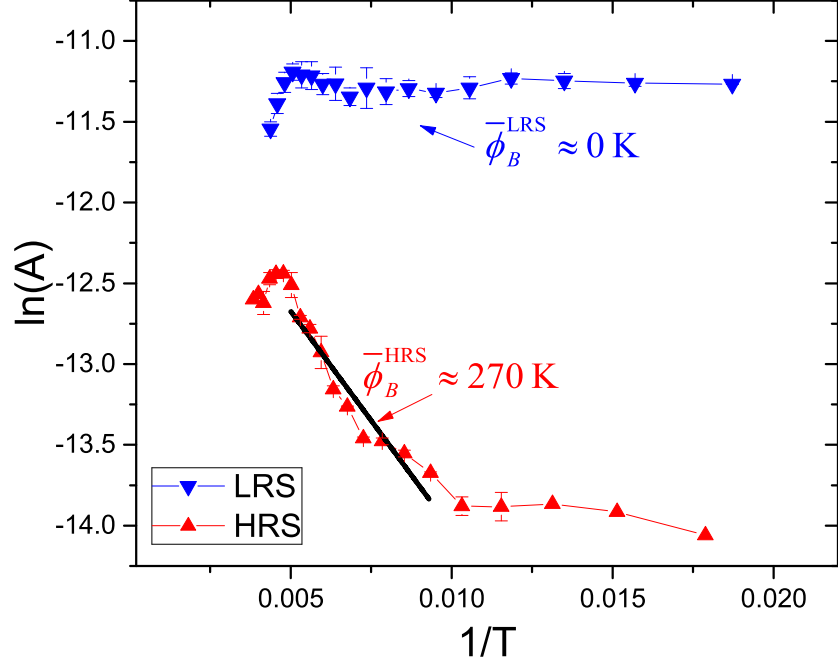


FIG. 9: Semilogarithmic plot of the A parameter as a function of $1/T$ for the LRS and HRS. $\bar{\phi}_t$ is the mean energy of the carrier's traps, which is obtained from the linear dependence as stated from Eq. 2 (see the line for the HRS data).

ceramic YBCO/Au devices (700-1200 K). [15]

In the case of the LRS, the obtained value of $\bar{\phi}_t$ is close to 0 K, although it should be non null as the non-linear behavior is still observed for this state ($\gamma > 1$), indicating the existence of shallow traps. Interestingly, in the HRS for $T \lesssim 90$ K, also $\bar{\phi}_t \rightarrow 0$ K, in accordance to the appearance of the superconducting state in optimally doped YBCO.

The extrapolation of the linear dependence for high temperatures, which corresponds to \tilde{A}_{PF} , gives similar values for both states, indicating that the main effect of the RS over the PF conduction is related to the variation of the trap energy $\bar{\phi}_t$.

For $T \geq 220$ K, both states show an anomalous behavior for the A parameter, which is reproduced both lowering and raising temperature without hysteresis. This feature was observed in several samples, sometimes making difficult for this temperature range to find a good fit of the experimental IV curves, determining as a consequence a noisy A parameter. Interestingly, at 200-250 K, partially oxygenated YBCO shows a phase transformation related to the reordering of oxygen atoms in the Cu-O basal planes, which softens its elastic properties. [39, 40] As the pulsing treatments that generate the RS modifies the number

of oxygen vacancies particularly in these planes, the appearance of this transition would then be expected. Although this phase transformation may generate misfitting domains due to non-elastic accommodations, the fact that no hysteresis is observed in the A parameter on cooling and heating indicates that the anomaly observed may be related to a dynamical property which affects the carrier's mobility. As this phase transformation was characterized as relatively slow, evolving during several thermal cycles, our transport measurements may result sensitive to this evolution in the time scale of our experiments.

These results point out to a scenario of high inhomogeneity in terms of oxygen concentration in the interfacial YBCO, with the coexistence of insulating zones ($x \simeq 6$), dominated by a VRH type transport and with the presence of PF traps, with a minority metallic phase, which may even be superconducting ($x \simeq 7$).

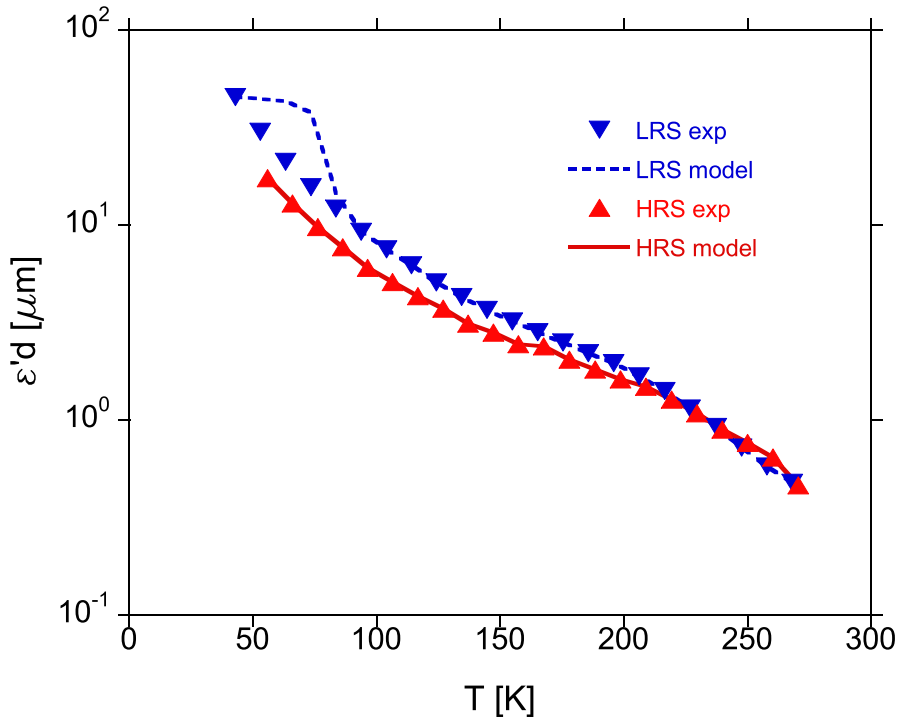


FIG. 10: Temperature dependence of $\epsilon'd$ for the LRS and HRS, derived from the B fitting-parameter by using Eq. 2. Lines are fits obtained by considering the model described by Eq. 8.

In this context of metallic zones embedded in an insulating matrix, the formation of thin (nanometric) capacitive layers in the interfacial zone should be expected. This will

lead to the Maxwell-Wagner (MW) effect [20], which amplifies the dielectric response of the device as well as its temperature dependence, eventually giving rise to an extrinsic colossal dielectric constant. [21] As this effect would not be caused solely by the metallic contact between Au/YBCO but is related to the inhomogeneities of the oxygen distribution in the YBCO interfacial zone, it can be viewed as intrinsic to this complex oxide, where the oxygen concentration can be varied spatially in an inhomogeneous way, generating this particular mixture of zones with different conductivities, acting as parallel-plate capacitors with very small plate distances.

As previously shown [21], this framework can be described by a simple equivalent circuit consisting in two layers connected in series: one for the interfacial zone (i) and the other for the bulk (B). Both zones of the same area and with a total width $d_T = d_i + d_B$. Each zone having a relative real part of the dielectric constant $\epsilon_{i,B}$ and represented by a conductance $G_{i,B}$ in parallel with a capacitance $C_{i,B}$. This configuration leads to the following expressions for the frequency (ω) dependence of the equivalent real dielectric constant (ϵ'), the relaxation time (τ), and the capacitance at high and low frequencies [$C(\infty)$ and $C(0)$, respectively]:

$$\epsilon'(\omega) = \epsilon'_\infty + \frac{\epsilon'_s - \epsilon'_\infty}{1 + (\omega \tau)^2} ; \quad \tau = \frac{C_i + C_B}{G_i + G_B} \quad (4)$$

$$C(\infty) = \frac{C_i C_B}{C_i + C_B} ; \quad C(0) = \frac{C_i G_B^2 + C_B G_i^2}{(G_i + G_B)^2} \quad (5)$$

where ϵ_s and ϵ_∞ are the static and the high frequency (ω) limit of $\epsilon'(w)$, respectively.

It can be noted that if $G_B \gg G_i$ and $C_i \gg C_B$ (which is the case if i is an insulating dielectric layer) and the intrinsic dielectric constant of each zone (i,B) varies slowly with temperature, the following approximations can be done:

$$\tau(T) \simeq \frac{C_i}{G_B} \sim G_B^{-1}(T) = R_B(T) ; \quad C(\infty) \simeq C_B ; \quad C(0) \simeq C_i. \quad (6)$$

If $R_B(T)$ has a metallic-like dependence, then $\tau(T)$ decreases with decreasing T and concomitantly ϵ' , measured at a fixed frequency, should increase (see Eq. 4).

Fig. 10 shows the temperature dependence of the dielectric response for both resistance states, extracted from the fitting parameter B , plotted as $\epsilon' d$ (which is essentially the temperature dependence of ϵ' with the assumption that d is temperature independent). From these results, it can be inferred that ϵ' increases with decreasing temperature. This behavior

is contrary to the one reported for oxygen poor YBCO ($x \simeq 6$) [35, 41], but fits very well in the MW scenario that we have described. Notice that $\epsilon' d$ is higher for the LRS than for the HRS. This result is in full agreement with the expected from the MW effect insofar as the interfacial zone is not short-circuited by the conductive phase.

This result is quite similar to the one reported for the magnetic-field-dependent dielectric constant of $\text{La}_{2/3}\text{Ca}_{1/3}\text{MnO}_3$ [42], where in the phase separation scenario of the manganites, the magnetic field favors the conversion of insulating regions into conducting ones, increasing the mixture that potentiates the MW effect, until a maximum is reached at the Curie temperature, when the metallic phase becomes the main one.

In this context, the observed increase of ϵ' with decreasing temperature is associated with the temperature dependence of the dielectric relaxation time $[\tau(T)]$ for a fixed measuring frequency (ω), indicating that ϵ' is evolving from ϵ'_∞ to ϵ'_s as stated in Eq. 4. This means that at a certain temperature (T_p) the experimental characteristic time equals the characteristic relaxation time:

$$\omega \simeq \frac{1}{C_i(T_p)R_B(T_p)}, \quad (7)$$

and by assuming that C_i is slightly temperature dependent in comparison with R_B , Eq. 4 can be rewritten as:

$$\epsilon'(T) \simeq \epsilon'_\infty + \frac{\epsilon'_s - \epsilon'_\infty}{1 + \left[\frac{R_B(T)}{R_B(T_p)}\right]^2}. \quad (8)$$

This two layer interface-equivalent circuit can be easily associated with the one we propose to describe our IV characteristics: it would only demand that the PF element acts as a resistor, which is the case if a constant current is used for its measurements, and to associate $R_B(T)$ with $R_S(T)$, that is easily fulfilled since the bulk resistance of YBCO $R_b \ll R_S$. In this way, the temperature dependence of $\epsilon' d$ presented in Fig.10 can be fitted by considering Eq. 8 with the $R_S(T)$ data presented in Fig. 7 as $R_B(T)$ and by determining $\epsilon_s d$, $\epsilon_\infty d$ and $R_b(T_p)$ as fitting parameters.

An excellent fit is obtained (see the lines shown in Fig.10). The model deviates from the experimental parameter for the LRS when the superconducting transition of $R_S^{LRS}(T)$ occurs, probably as a consequence of a sudden increase in C_i , which contradicts the assumptions made of its slight temperature dependence. The obtained parameters are listed in Table 1.

A crude estimation of d , and thus of ϵ'_∞ , ϵ'_s and ϵ'_i can be made by considering the

TABLE I: Parameters derived from fitting the temperature dependence of ϵd by considering Eq. 8 and the obtained values of $R_b(T)$.

State	$\epsilon'_\infty d$ (μm)	$\epsilon'_S d$ (μm)	$R_S(T_p)$ (Ω)	T_p (K)
HRS	0.1	22.8	4.7	70
LRS	0.14	47.3	3.9	60

approximate values of the equivalent capacitance at low and high frequencies (see Eq. 6), by assuming that $d \sim d_i \sim d_B \sim d_T/2$ and that ϵ'_B can be associated with the dielectric constant of YBCO, which ranges from 5 to 40, depending on its granularity. [38, 43, 44] In that case it can be shown that:

$$d_T \simeq \frac{\epsilon'_\infty d}{\epsilon'_B} ; \quad \epsilon'_i \simeq \frac{\epsilon'_S d}{d_T}, \quad (9)$$

which gives the possibility to estimate the mentioned values for the HRS and the LRS, as summarized in Table 2.

TABLE II: Estimation of d_T , d , ϵ'_∞ , ϵ'_i and ϵ'_S derived from Eq. 6 and 9 and the values reported in Table 1.

State	d_T (nm)	d (nm)	ϵ'_∞	ϵ'_i ($\times 10^3$)	ϵ'_S ($\times 10^3$)
HRS	2.5-20	1.3-10	10-80	1-9	2.3-18
LRS	3.5-28	1.8-14	10-80	1.7-14	3.4-27

It can be observed that the width of the whole interface region (d_T) is of the order of 10 nm and increases when switching the device from HRS to LRS. This value is in accordance to other estimations in YBCO [18] as well as in other RRAM devices based on the oxygen diffusion mechanism. [45]

The large dielectric constant of the insulating layer ϵ'_i is in the range of the one reported for oxygen depleted YBCO [35], although these published colossal values can be affected by the extrinsic effect already mentioned and associated with interfaces. In spite of the fact that we have shown that the MW formalism gives an excellent description of the derived

dielectric behavior of the inhomogeneous interfacial region of YBCO, the high values of ϵ'_i can not be the result of the formation of tiny parallel capacitors with an ordinary dielectric constant in the 10-40 range, as this would require that their distance between metallic plates to be $\leq 1\text{\AA}$. In this way, it should be envisioned an intrinsic dielectric constant of this region much higher than the expected for regular dielectric oxides.

As a final remark, It should be noted that we have used a model that propose an effective dielectric constant associated with the whole interfacial zone, composed by two different material (i, B), which reproduce the temperature dependence of the dielectric constant extracted from the PF conduction. However, it is natural to associate the interfacial region i to the one where the PF conduction is developed, so that the dielectric constant extracted from the PF conduction (see Fig. 10) should be more likely related to ϵ'_i rather than to ϵ' . The very good reproduction of its temperature dependence by considering the two layer model leads us to think that instead of having two well separated layers, these may be distributed randomly in a set of equivalent multilayers, which behave identically from the dielectric point of view [20] but are averaged to the MW derived values by the electrical carriers in a relevant distance like the localization length. Further studies are needed to determine the origin of the dielectric behavior of these interfaces.

IV. CONCLUSIONS

The electrical transport properties of Au / YBCO films were studied by measuring the temperature dependence of their I-V curves in the HRS and the LRS. Its analysis reveals the existence of a complex scenario, where an interfacial zone composed by two layers can be distinguished from the bulk YBCO. In the first layer, the observed electronic localization plus a non-linear behavior based on the PF effect is consistent with the presence of YBCO6, while the extracted temperature dependence of the dielectric response would also require, in terms of the MW effect, the existence of a minority metallic YBCO. This scenario, mainly generated by the electric-field-assisted drift of oxygen produced to achieve the RS of the device, depicts an inhomogeneous distribution of the oxygen content in this interfacial zone, with a higher (lower) proportion of YBCO7 in a matrix of YBCO6 in the LRS (HRS). In the second layer, a series resistor associated with a percolating metallic-like conductive YBCO phase ensures a conducting path through small channels with the bulk YBCO zone.

The dielectric constant extracted from the PF conduction follows a Debye relaxation law, consistent with a MW scenario, but requiring a much higher intrinsic dielectric constant for the insulating layer, outside the usual value for oxides.

V. ACKNOWLEDGEMENTS

We would like to acknowledge financial support by CONICET Grant PIP 11220150100653CO, PICT 2017-0984 and UBACyT 20020170100284BA (2018-2020). Jenny and Antti Wihuri Foundation is also acknowledged for financial support. We are indebted to A. Schulman, M. Boudard and C. Jiménez for fruitful discussions in an early stage of this research. We thank D. Giménez, E. Pérez Wodtke and D. Rodríguez Melgarejo for their technical assistance.

-
- [1] J Borghetti, G S Snider, P J Kuekes, J J Yang, D R Stewart, and R. S Williams. memristive switches enable stateful logic operations via material implication. *Nature*, 464:873–876, 2010.
 - [2] Sung Hyun Jo, Ting Chang, Idongesit Ebong, Bhavitavya B. Bhadviya, Pinaki Mazumder, and Wei Lu. Nanoscale memristor device as synapse in neuromorphic systems. *Nano Letters*, 10(4):1297–1301, 2010.
 - [3] E. Zamanidoost F. Alibart and D. B. Strukov. Pattern classification by memristive crossbar circuits using ex situ and in situ training. *Nature Communications*, 4:2072, 2013.
 - [4] Pablo Stoliar, Julien Tranchant, Benoit Corraze, Etienne Janod, Marie-Paule Besland, Federico Tesler, Marcelo Rozenberg, and Laurent Cario. A leaky-integrate-and-fire neuron analog realized with a mott insulator. *Advanced Functional Materials*, 27(11):1604740, 2017.
 - [5] M. J. Rozenberg, M. J. Sánchez, R. Weht, C. Acha, F. Gomez-Marlasca, and P. Levy. *Phys. Rev. B*, 81:115101, 2010.
 - [6] A. Schulman, M. J. Rozenberg, and C. Acha. *Phys. Rev. B*, 86:104426, 2012.
 - [7] T. Plecenik, M. Tomasek, M. Belogolovskii, M. Truchl, M. Gregor, J. Noskovic, M. Zahoran, T. Roch, I. Boylo, M. Spankova, S. Chromik, P. Kus, and A. Plecenik. *J. Appl. Phys.*, 111:056106, 2012.
 - [8] C. Acha and M. J. Rozenberg. *J. Phys.: Condens. Matter*, 21:045702, 2009.

- [9] C. Acha. *Physica B*, 404:2746, 2009.
- [10] A. Plecenik, M. Tomasek, T. Plecenik, M. Truchly, J. Noskovic, M. Zahoran, T. Rocha, M. Belogolovskii, M. Spankova, S. Chromik, and P. Kus. *Appl. Surface Science*, 256:5684, 2010.
- [11] C. Acha. *J.Phys.D: Appl.Phys.*, 44:345301, 2011.
- [12] A. Schulman and C. Acha. *J. Appl. Phys.*, 114:243706, 2013.
- [13] A. Schulman and C. Acha. *MRS Proceedings*, 1337:q10–07, 2011.
- [14] A. Palau, A. Fernandez-Rodriguez, J. C. Gonzalez-Rosillo, X. Granados, M. Coll, B. Bozzo, R. Ortega-Hernandez, J. Su, N. Mestres, X. Obradors, and T. Puig. *ACS Applied Materials & Interfaces*, 10(36):30522–30531, 2018.
- [15] A. Schulman, L. F. Lanosa, and C. Acha. *Journal of Applied Physics*, 118:044511, 2015.
- [16] J. Waśkiewicz and J. Golebiowski. *Przegląd Elektrotechniczny*, 91:313–317, 2015.
- [17] M. Truchly, T. Plecenik, E. Zhitlukhina, M. Belogolovskii, M. Dvoranova, P. Kus, and A. Plecenik. Inverse polarity of the resistive switching effect and strong inhomogeneity in nanoscale ybco-metal contacts. *Journal of Applied Physics*, 120(18):185302, 2016.
- [18] J. Waśkiewicz. *Przegląd Elektrotechniczny*, 94:99–103, 2018.
- [19] N A Tulina, A N Rossolenko, I M Shmytko, A A Ivanov, V V Sirotkin, I Yu Borisenko, and V A Tulin. *Superconductor Science and Technology*, 32(1):015003, nov 2018.
- [20] A.R. Von Hippel. *Dielectrics and Waves*, pages 228–234. John Wiley and Sons, 1962.
- [21] P. Lunkenheimer, S. Krohns, S. Riegg, S.G. Ebbinghaus, A. Reller, and A. Loidl. *The European Physical Journal Special Topics*, 180:61, 2010.
- [22] M.Z. Khan, E. Rivasto, J. Tikkanen, H. Rijckaert, M. Malmivirta, M. O. Liedke, M. Butterling, A. Wagner, H. Huhtinen, I. Van Driessche, and P. Paturi. Enhanced flux pinning isotropy by tuned nanosized defect network in superconducting $\text{YBa}_2\text{Cu}_3\text{O}_{6+x}$ films. *Sci Rep*, 9(4):15425, 2019.
- [23] H. Huhtinen, J. Järvinen, R. Laiho, P. Paturi, and J. Raittila. *Journal of Applied Physics*, 90(3):1521–1528, 2001.
- [24] P. Paturi, M. Peurla, K. Nilsson, and J. Raittila. Crystalline orientation and twin formation in YBCO thin films laser ablated from a nanocrystalline target. *Superconductor Science and Technology*, 17:564, 2004.
- [25] M. Peurla, H. Huhtinen, Y. Y. Tse, J. Raittila, and P. Paturi. Structural properties of

- ybco thin films deposited from different kinds of targets. *IEEE Transactions on Applied Superconductivity*, 17:3608–3611, 2007.
- [26] S. M. Sze and K. K. Ng. Physics of semiconductor devices. chapter 3-4. John Wiley & Sons, 2007.
- [27] F-Ch Chiu. *Advances in Materials Science and Engineering*, 2014:578168, 2014.
- [28] C Acha. Graphical analysis of current-voltage characteristics in memristive interfaces. *Journal of Applied Physics*, 121(13):134502, 2017.
- [29] C. Acha, A. Schulman, M. Boudard, K. Daoudi, and T. Tsuchiya. *Applied Physics Letters*, 109:011603, 2016.
- [30] W. Román Acevedo, C. Acha, M. J. Sánchez, P. Levy, and D. Rubi. *Applied Physics Letters*, 110:053501, 2017.
- [31] N Ghenzi, M Barella, D Rubi, and C Acha. Adaptive threshold in TiO₂-based synapses. *Journal of Physics D: Applied Physics*, 52(12):125401, jan 2019.
- [32] I.P. Batra, E. Tekman, and S. Ciraci. Theory of schottky barrier and metallization. *Progress in Surface Science*, 36(4):289 – 361, 1991.
- [33] A. Matsushita, T. Oguchi, K. Kimura, T. Matsumoto, T. Hatano, K. Ogawa, and S. Takayanagi. *Jap. J. Appl. Phys.*, 26:L1953, 1987.
- [34] F. P. Milliken, T. Doderer, R. H. Koch, and C. C. Tsuei. *Phys. Rev. B*, 62:9143, 2000.
- [35] C. M. Rey, H. Mathias, L. R. Testardi, and S. Skirius. High dielectric constant and nonlinear electric response in nonmetallic yba₂cu₃o_{6+δ}. *Phys. Rev. B*, 45:10639–10646, 1992.
- [36] B. I. Shklovskii and A. L. Efros. *Electronic properties of doped semiconductors*. Springer-Verlag, 1984.
- [37] N. F. Mott. *Metal-insulator transitions*. Taylor & Francis, 1990.
- [38] J. Mannhart. *Supercond. Sci. Technol.*, 9(4):49, 1996.
- [39] G. Cannelli, R. Cantelli, F. Cordero, G. A. Costa, M. Ferretti, and G. L. Olcese. *Europhys. Lett.*, 6:271, 1988.
- [40] G Cannelli, R Cantelli, F Cordero, and F Trequattrini. *Superconductor Science and Technology*, 5(4):247–257, apr 1992.
- [41] G. A. Samara, W. F. Hammetter, and E. L. Venturini. Temperature and frequency dependences of the dielectric properties of YBa₂Cu₃O_{6+x} (x ≈ 0). *Phys. Rev. B*, 41:8974–8980, 1990.

- [42] J. Rivas, J. Mira, B. Rivas-Murias, A. Fondado, J. Dec, W. Kleemann, and M. A. Señaris-Rodríguez. *Applied Physics Letters*, 88(24):242906, 2006.
- [43] J. Humliek, J. Kircher, H.-U. Habermeier, M. Cardona, and A. Rselser. *Physica C: Superconductivity*, 190(4):383 – 395, 1992.
- [44] M.A. Navacerrada, M.L. Lucia, and F. Sanchez-Quesada. *Physica C: Superconductivity*, 483:195 – 200, 2012.
- [45] Y. Aoki, C. Wiemann, V. Feyer, H-S. Kim, C. M. Schneider, H. Ill-Yoo, and M. Martin. *Nature Communications*, 5:3473, 2014.